

THE IONIZATION IN THE WINDS OF O STARS AND THE DETERMINATION OF MASS-LOSS RATES FROM ULTRAVIOLET LINES

HENNY J. G. L. M. LAMERS,^{1,2,3} STEPHAN HASER,⁴ ALEX DE KOTER,⁵ AND CLAUS LEITHERER¹

Received 1998 May 8; accepted 1998 December 16

ABSTRACT

Empirical ionization fractions of C IV, N V, Si IV, and empirical ionization plus excitation fractions of C III* and N IV* in the winds of 34 O stars and one B star have been derived. We combine the mass-loss rates derived from radio measurements and H α with the line fitting of ultraviolet resonance lines and subordinate lines using the Sobolev plus exact integration (SEI) method. The dependence of the empirical ionization fractions, $\langle q \rangle$, on the stellar effective temperature and on the mean wind density is discussed. This sets constraints for the models of ionization in the winds of hot stars. The ionization and excitation fractions can be expressed in terms of an *empirical* radiation temperature. This radiation temperature scales with T_{eff} , and we derive empirical relations for T_{rad} as a function of T_{eff} . The radiation temperatures are on the order of 0.5–0.9 T_{eff} , with significant differences between the ions. The derived relations between the ionization fractions and the stellar parameters have an uncertainty of 0.2 dex for Si IV, N V, and C III*, and about 0.26 dex for N IV*. For C IV, we can only derive an expression for the mean ionization fraction in the wind if the mass-loss rate is small, $\dot{M} < 10^{-6} M_{\odot} \text{ yr}^{-1}$, because the C IV lines are usually saturated for higher mass-loss rates. The resulting expressions for T_{rad} can be used to derive the mass-loss rates from studies of ultraviolet P Cygni profiles in the range of stellar parameters studied here: $30,000 \text{ K} \lesssim T_{\text{eff}} \lesssim 50,500 \text{ K}$, $5.2 \lesssim \log L/L_{*} \lesssim 6.4$, and $-7.5 M_{\odot} \lesssim \log \dot{M} \lesssim -4.6 M_{\odot} \text{ yr}^{-1}$. An accuracy of about a factor of 2 or better can be reached, depending on the lines that are used and the accuracy of the line fits and the stellar parameters. The Si IV lines give the most reliable mass-loss rates, because the abundance is about the same for all O stars, the lines saturate only for high mass-loss rates, the doublet lines only partly overlap, and the mass-loss rate is proportional to the square root of the column density. The radiation temperature of N V shows a surprisingly strict relation with T_{eff} , with a scatter of only $\Delta T_{\text{rad}}/T_{\text{eff}} = 0.01$. The mass-loss rate cannot be derived from the N V lines, because the column density of the N V ions in the wind is independent of \dot{M} . A consistency check and a test of the method for the stars HD 14749 and HD 190429 show that the mass-loss rate derived from the UV lines with the ionization fractions of this paper agree very well with the mass-loss rate derived from new radio flux measurements.

Subject headings: stars: atmospheres — stars: early-type — stars: mass loss — ultraviolet: stars

1. INTRODUCTION

Ultraviolet resonance lines of abundant ions are the most sensitive indicators of mass loss from early-type stars: mass-loss rates (\dot{M}) as small as 10^{-9} to $10^{-10} M_{\odot} \text{ yr}^{-1}$ can easily be detected by P Cygni profiles or violet absorption wings of UV resonance lines and subordinate lines from low excitation levels of abundant ions. The major UV lines that indicate mass loss from O stars at $\lambda > 1150 \text{ \AA}$, i.e., the wavelength region accessible to *IUE*, *Hubble Space Telescope* (*HST*), and the Hopkins Ultraviolet Telescope (*HUT*), are the resonance lines of N V (1240 \AA), C IV (1550 \AA), Si IV (1400 \AA), and the lines from the excited levels of C III* (1176 \AA), N IV* (1718 \AA), and He II* (1640 \AA).⁶

Unfortunately, quantitative determination of the mass-loss rates from UV lines is very difficult and uncertain. This is because only *unsaturated lines* can be used for the determination of \dot{M} . The observed lines are either saturated (in which case they only indicate a lower limit of \dot{M}), or they are from trace ions, if $\dot{M} > 10^{-8} M_{\odot} \text{ yr}^{-1}$. The determination of \dot{M} from trace ions of abundant elements requires large and usually uncertain corrections for the ionization in the winds. Such corrections can easily be on the order of 10^2 to 10^3 , with an uncertainty of about an order of magnitude. This problem has hampered the determination of mass-loss rates of early-type stars from UV lines over many years.

The mass-loss rates can be derived more accurately from the radio and infrared free-free emission, from the wind emission of H α , and, for the hotter Of stars, also from the wind emission of the He II line at 1640 \AA . However, these methods can only be applied to stars with mass-loss rates on the order of $10^{-6} M_{\odot} \text{ yr}^{-1}$ or higher for radio data, $10^{-7} M_{\odot} \text{ yr}^{-1}$ or higher for H α , and $10^{-5} M_{\odot} \text{ yr}^{-1}$ or higher for the He II line. For lower rates, the UV lines provide the only observable indication of mass loss from hot stars. Therefore, a knowledge of the ionization fractions is crucial for determining \dot{M} from these stars.

The uncertainty in the ionization fractions is partly due to the effects of shocks in the wind, partly due to the uncer-

¹ Space Telescope Science Institute, 3700 San Martin Drive, Baltimore, MD 21218.

² Astronomical Institute, Princetonplein 5, NL-3584 CC Utrecht, The Netherlands.

³ SRON Laboratory for Space Research, Sorbonnelaan 2, NL-3584 CA Utrecht, The Netherlands.

⁴ Universitäts-Sternwarte Muenchen, Scheinerstrasse 1, D-8000, Munich 80, Germany.

⁵ Astronomical Institute Anton Pannekoek, University of Amsterdam, Kruislaan 403, NL-1098 SJ, Amsterdam, The Netherlands.

⁶ Throughout this paper we indicate the ions with subordinate lines by a superscript asterisk.

tainty in the UV line blocking by numerous metal lines, and partly due to the uncertainty in the photospheric ionizing flux at $\lambda < 912 \text{ \AA}$. The effect of shocks on the ionization can in principle be calculated, but in practice this is hampered by our lack of reliable quantitative knowledge about these shocks. The far-UV blocking of the photospheric flux is difficult to calculate, because it involves the effects of millions of lines, many of them in non-LTE. For a discussion of the different effects on the ionization in the wind, we refer the reader to the paper by Pauldrach et al. (1994).

This uncomfortable situation, with its large uncertainties in the mass-loss determinations from UV lines, may improve in the future in three ways: (1) by improved ionization calculations; (2) by extension of the observable wavelength range down to the Lyman limit by the *Far Ultraviolet Spectroscopic Explorer (FUSE)* satellite, so that unsaturated resonance lines from the dominant ionization stages of low-abundance elements can be observed; and (3) by using empirical ionization fractions that can be derived from stars with known mass-loss rates from radio fluxes and H α .

Approach 1.—A first attempt to calculate the shocks, the resulting ionization, and the X-ray spectrum has been made by MacFarlane et al. (1993) for the star ζ Pup, by MacFarlane, Cohen, & Wang (1994) for the stars 9 Sgr, 15 Mon, μ Col, τ Sco, λ Sco, and α Pav, and by Pauldrach et al. (1994) for the stars ζ Pup and Melnick 42. Their results are both encouraging and discouraging. On the one hand, they suggest the possibility of computing the ionization in the winds of O stars in the future, but on the other hand, they show the complexity of the problem. For instance, Pauldrach et al. (1994) had to adjust a number of free parameters to match the calculated spectrum with the observed one, using not only the usual stellar parameters T_{eff} , R_* , M_* and the abundances, but also the temperature and mass fraction of the shocked gas and the brightness temperature of the photosphere in three far-UV wavelength regions. Although the agreement between the final calculated spectrum and the observations is impressive, the required adjustment of these extra five parameters shows that at present it is not possible to calculate the O-star wind ionization from first principles.

Approach 2.—The extension of the wavelength range down to the Lyman limit allows the detection of the UV resonance lines of, e.g., P v, S iv, and S vi (see Snow & Morton 1976), which are not saturated even when they are the dominant stage of ionization.

Approach 3.—Improved analysis of UV line profiles, e.g., with the Sobolev plus exact integration (SEI) method (Lamers, Cerrutti-Sola, & Perinotto 1987), gives accurate determinations of the optical depths, $\tau(v)$, as a function of the velocity in the wind. Mass-loss rates derived from radio fluxes or from H α are now available for about 50 O stars (Lamers & Leitherer 1993; Puls et al. 1995). The combination of the results from UV line fitting with these mass-loss rates provides *empirical* ionization fractions in a grid of O stars of different luminosities and spectral types.

In this paper we apply the third method. We use UV line-fitting results of Groenewegen & Lamers (1989; hereafter GL), and Haser (1995), which are based on the SEI method, to derive the Sobolev optical depth as a function of wind velocity. This analysis also gives the velocity laws in the winds. We adopt the mass-loss rates from radio fluxes

and from H α for the same stars for which the UV lines were analyzed. In this way we derive the empirical ionization fractions for 34 O stars and one B star.

Similar studies have been made in the past by Lamers, Gathier, & Snow (1980) and by Howarth & Prinja (1989). However, these studies were based on simple line fitting of the UV profiles with the Sobolev method, which does not take into account the presence of chaotic motions (“turbulence”) in the winds. Lamers et al. (1987) have demonstrated that this can lead to significant errors in the derived column densities and in the resulting empirical ionization. We will show later that indeed the ionization fractions derived in this paper differ significantly from the results of the older studies.

The empirical ionization fractions derived in this paper are valid for the range of stellar parameters for which independent mass-loss determinations based on H α and on the radio flux are available, i.e., for hot stars with $-7.5 M_{\odot} \text{ yr}^{-1} \lesssim \log \dot{M} \lesssim -4.6 M_{\odot} \text{ yr}^{-1}$. They serve two purposes: (1) The ionization fractions will constrain the models for the ionization in the winds of hot stars. Improved models of the wind ionization will also more accurately predict the ionization fractions of stars with smaller mass-loss rates, so that for less luminous stars the smaller mass-loss rates can be derived from the UV lines. (2) Even for hot luminous stars with high mass-loss rates, the UV lines still offer the only way to derive mass-loss rates if the stars are too distant to have a detectable radio flux (typically $d \gtrsim 3 \text{ kpc}$) and if the stars have strongly variable or abnormal H α profiles.

In § 2 we introduce the program stars and their parameters. In § 3 we describe the derivation of the mean ionization fractions from UV lines of stars with known mass-loss rates. In § 4 we derive empirical ionization fractions for N v, C iv, Si iv, C iii*, and N iv*, and we discuss their dependence on T_{eff} and the wind density. In § 5 we derive empirical relations for ionization fractions. In § 6 we give the formulae for deriving mass-loss rates from the UV lines. In § 7 we apply these relations for a consistency check by calculating \dot{M} from the column densities and comparing it with the mass-loss rates derived from the radio flux or from H α . The results are also compared with mass-loss rates from new radio data of three stars. The discussion and conclusions are given in § 8.

2. PROGRAM STARS

2.1. Stellar Parameters

The stars are listed in Table 1. For these stars, GL and Haser (1995) have derived reliable fits to the UV wind lines with the SEI method, and the mass-loss rates are known (see below). We did not include the star ζ Per in this study, although its UV lines were studied by GL and Haser and the mass-loss rate was derived from H α by LL and by Puls et al. (1995). The mass-loss rate of this star and the stellar parameters are very uncertain (Herrero et al. 1992; Puls et al. 1995) because the wind is highly variable, especially in the lower layers where H α is formed. We also eliminated the few stars that have an exceptionally slow velocity law of $\beta \geq 1.5$ derived from the H α profile by Puls et al. (1995). It is not clear why these stars deviate from the majority of the O stars. The slow velocity is derived from the excess of H α emission at low velocities. This might indeed be due to an abnormally slow velocity law, but other explanations are also possible, e.g., the presence of significant clumping in the

TABLE 1
PROGRAM STARS

HD (1)	Name (2)	Spectral Type (3)	T_{eff} (10^3 K) (4)	$\log L$ (L_{\odot}) (5)	R_* (R_{\odot}) (6)	v_{∞} (km s^{-1}) (7)	β (8)	$\log \dot{M}$ ($M_{\odot} \text{ yr}^{-1}$) (9)	$\log \langle \rho \rangle$ (g cm^{-3}) (10)	References for Stars (11)	References for \dot{M} (12)
93129A	O3 If*	50.5	6.37	20	3200	0.70	-4.66 ± 0.18	-12.85	1	1
93250	O3 V(ff)	50.5	6.28	18	3250	0.70	-5.31 ± 0.18	-13.51	1	1
303308	O3 V(ff)	48.0	5.84	12	3100	0.70	-5.68 ± 0.20	-13.42	1	1
15570	O4 If ⁺	42.4	6.14	22	2800	0.80	-5.33 ± 0.18	-13.62	2	7
66811	ζ Pup	O4 I(nf)	42.0	6.01	19	2350	0.80	-5.62 ± 0.15	-13.71	3	7
190429A	O4 If ⁺	42.4	6.06	20	2300	0.80	-4.86 ± 0.18	-12.97	4	4
46223	O4 V(ff)	46.4	5.70	11	2800	0.80	-5.68 ± 0.19	-13.36	4	4
164794	9 Sgr	O4 V(ff)	46.4	6.02	16	2950	0.80	-5.46 ± 0.20	-13.48	4	4
14947	O5 If ⁺	43.5	5.92	16	2350	1.00	-5.12 ± 0.18	-13.18	1	1
15558	O5 III(f)	48.0	6.36	22	2800	0.70	-5.14 ± 0.21	-13.35	1	1
15629	O5 V(ff)	47.0	5.95	14	3000	0.70	-6.12 ± 0.19	-13.99	1	1
93204	O5 V(ff)	44.2	5.48	9	2800	0.80	-6.55 ± 0.30	-14.09	4	8
210839	λ Cep	O6 I(n)fp	38.0	5.83	19	2250	0.70	-5.68 ± 0.15	-13.67	1	7
101190	O6 V(ff)	42.2	5.74	14	2900	0.80	-6.05 ± 0.30	-13.95	4	8
163758	O6.5 Iaf	37.2	5.96	23	2200	0.80	-5.21 ± 0.30	-13.43	4	8
190864	O6.5 III(f)	41.0	5.71	14	2500	0.70	-5.82 ± 0.19	-13.61	5	1
101436	O6.5 V	41.2	5.60	12	2800	0.80	-6.23 ± 0.30	-14.02	4	8
193514	O7 Ib(f)	38.0	5.87	20	2200	1.00	-5.38 ± 0.20	-13.59	5	1
47839	15 Mon	O7 V(ff)	39.5	5.33	10	2150	0.70	-6.19 ± 0.31	-13.60	5	4
217086	O7 Vn	40.0	5.39	10	2550	0.70	-6.70 ± 0.20	-14.22	5	1
188001	9 Sge	O7.5 Iaf	34.0	5.86	24	1800	0.70	-5.11 ± 0.18	-13.30	4	4
203064	68 Cyg	O7.5 III:n(ff)	37.5	5.55	14	2500	0.70	-5.92 ± 0.20	-13.70	5	1
151804	O8 Iaf	34.0	6.14	34	1600	0.80	-5.00 ± 0.17	-13.42	4	7
36861	λ Ori	O8 III(ff)	36.0	5.38	13	2400	0.80	-6.09 ± 0.31	-13.82	4	4
101413	O8 V	38.0	5.23	13	2900	0.80	-7.36 ± 0.30	-14.93	4	8
149404	O9 Ia	32.0	6.05	34	2400	1.00	-4.91 ± 0.15	-13.63	2	7
207198	O9 Ib-II	34.0	5.44	15	2150	1.00	-5.80 ± 0.20	-13.77	5	1
57061	O9 II	34.0	6.02	29	2200	1.00	-5.20 ± 0.15	-13.74	2	1
37043	ι Ori	O9 III	34.0	5.58	18	2450	0.80	-6.50 ± 0.18	-14.54	4	7
149757	O9 III	32.5	5.22	13	1550	1.00	-7.52 ± 0.30	-15.20	2	1
209975	19 Cep	O9.5 Ib	32.5	5.47	17	2050	1.00	-6.04 ± 0.20	-14.10	5	1
36486	δ Ori	O9.5 II	32.9	5.82	25	2100	0.70	-5.97 ± 0.15	-14.17	6	7
149038	μ Nor	O9.7 Iab	30.9	5.78	27	1750	0.80	-5.48 ± 0.18	-13.74	4	4
37742	ζ Ori	O9.7 Ib	30.9	5.90	31	2100	0.80	-5.60 ± 0.15	-14.06	4	7
37128	ϵ Ori	B0 Ia	28.0	5.80	34	1600	1.00	-5.39 ± 0.16	-13.93	4	7

REFERENCES.—(1) Puls et al. 1995; (2) Haser 1995; (3) Pauldrach et al. 1994, mass-loss rates from H α ; (4) Lamers & Leitherer 1993, mass-loss rates from H α , modified (see § 2.2); (5) Herrero et al. 1992; (6) Voels et al. 1989; (7) \dot{M} from radio (Lamers & Leitherer 1993); (8) Lamers & Cassinelli 1996, predicted mass-loss rate.

lower part of the wind or a nonspherical wind. Because of the uncertainty in the velocity law and hence in the density structure of these abnormal stars, they were excluded from this study.

The spectral types are from the catalog of C. D. Garmany (1995, private communication). They are based on several classification studies, mainly by N. Walborn. The stellar parameters T_{eff} , $\log L_*$, and R_* are from the non-LTE studies of these stars by Herrero et al. (1992), Pauldrach et al. (1994), Puls et al. (1995), and Voels et al. (1989). For the stars not studied by these authors, we adopted the relations between the stellar parameters and spectral types derived by LL on the basis of several non-LTE studies, mainly by the Munich group (see LL). The reference is indicated in column (11).

The program stars are plotted in the Hertzsprung-Russell diagram in Figure 1.

2.2. The Mass-Loss Rates

The mass-loss rates are from three sources. (1) The mass-loss rates derived from the radio free-free emission are considered to be the most accurate ones. Therefore, we adopted

these rates whenever possible. They were derived by LL from radio observations collected from the literature, using the stellar parameters derived from the non-LTE studies described above. (2) The mass-loss rates of many O stars have been derived from a very accurate analysis of the profiles of H α by Puls et al. (1995). (3) LL derived the mass-loss rates from the equivalent width of H α . Puls et al. (1995) have compared this method and its results with their own, more accurate analysis and have shown that there is a small systematic difference. This difference depends on the equivalent width of the wind contribution to H α . We applied this correction to the mass-loss rates derived by LL, based on Figure 19 of Puls et al. (1995). The correction to \dot{M} is about 0.16 dex, and it is largest for the lines with the strongest H α emission. The references for the adopted mass-loss rates are listed in Table 1, column (12). The uncertainty in the mass-loss rates is taken from the study of LL. The mass-loss rates derived by Puls et al. probably have a smaller uncertainty, but since these authors do not list these, we adopted the uncertainties estimated by LL as conservative limits.

Six stars in our sample do not have mass-loss rates derived from either the radio flux or H α ; these stars were

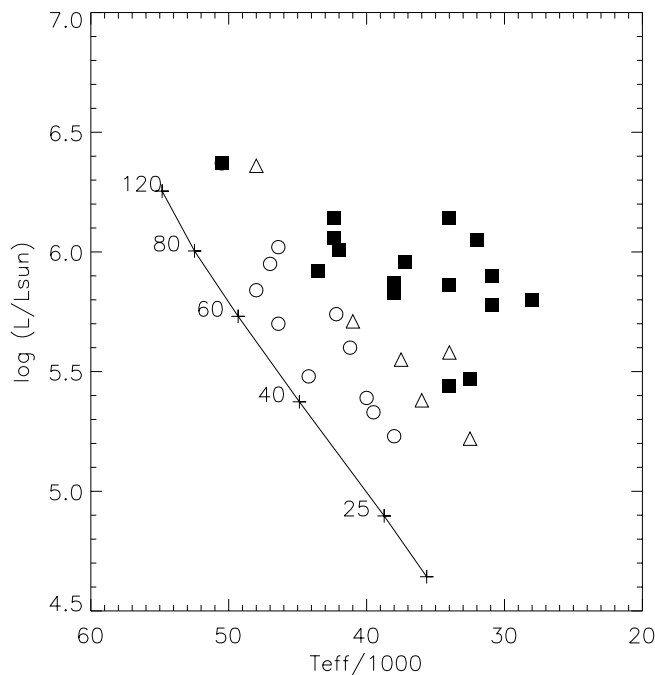


FIG. 1.—Location of the program stars in the Hertzsprung-Russell diagram. The location of the zero-age main sequence of Maeder (1990), with the corresponding masses, is indicated by the solid line. The different symbols indicate the luminosity classes: *open circles*, classes IV and V; *triangles*, classes II and III; *filled squares*, class I and Of stars.

included to ensure a sufficiently large sample of different spectral types. The mass-loss rates of these stars were calculated by means of the relation between \dot{M} and the stellar parameters derived by Lamers & Cassinelli (1996). For O stars, this relation is based on the mass-loss rates from the radio data and from the study of $H\alpha$ by Puls et al. (1995). The relation agrees approximately with the radiation-driven wind theory, apart from a systematic deviation found by LL and confirmed by Puls et al. Therefore, the rates are consistent with those used for the other stars in our sample. We adopt an uncertainty of a factor of 2 for these predicted mass-loss rates.

The terminal velocities, v_∞ , are from the detailed line fitting by Haser (1995). These values are in excellent agreement with those derived by GL and for a much larger sample of stars by Lamers, Snow, & Lindholm (1995), within about 100 km s^{-1} . The terminal velocities have an accuracy of about $100\text{--}150 \text{ km s}^{-1}$ (see the profile fits by GL and by Haser 1995). We assumed a β -type velocity law (see eq. [2] below) with values of β between 0.7 and 1.0 from Haser (1995), which agree with those of Groenewegen & Lamers (1989, 1991).

We define the mean density in the wind as the density at which $v = 0.5v_\infty$:

$$\langle \rho \rangle = \frac{\dot{M}}{4\pi r_{0.5}^2 v_\infty}, \quad (1)$$

where $r_{0.5}$ is the distance at which 50% of the terminal velocity has been reached. This is at $1.59R_*$ for a β -law with $\beta = 0.70$, and at $2.00R_*$ for $\beta = 1.0$. The values of $\langle \rho \rangle$ are listed in column (10) of Table 1.

Since we express the ionization in terms of $\langle \rho \rangle$ and T_{eff} , we have to verify that these two quantities are not corre-

lated with one another in our sample of stars. Figure 2 shows that indeed there is no such correlation, and that it is basically a triangular scatter diagram. This reflects the distribution of the stars in the H-R diagram, since the mass-loss rate increases with luminosity.

2.3. The Abundances

The empirical ionization fractions depend on the adopted abundances. The abundances of C and N can vary between those of OC stars, which have stronger than normal C lines, normal stars, and ON stars, which have stronger than normal N lines. Walborn (1976, 1988) proposed that OC stars have solar abundances, that “normal” O stars are slightly enriched in N, and that ON stars are strongly enriched in N and depleted in C, because of the appearance of nuclear products of the CN cycle at the surface. This suggestion has been supported by several abundance studies, e.g., Schönberner et al. (1988) and Lennon et al. (1991). These authors found an N/C ratio by number of about $2 \times$ solar for “normal” O main-sequence stars and $4 \times$ solar for the moderately N-deficient O supergiant κ Ori. Pauldrach et al. (1994) found that in ζ Pup, N is overabundant by a factor of 4 and C is underabundant by a factor of 0.35, so the N/C ratio is $11 \times$ solar.

We have excluded the well-established ON and OC stars, which have much larger abundance anomalies, from our sample. The only exceptions are the moderately N-deficient stars ζ Ori and ϵ Ori (Walborn 1976). The atmospheres of these stars are less enriched in N than those of the other stars. They also have a He abundance that is close to the solar value (e.g., Voels et al. 1989).

Based on these considerations, we adopted the following abundances: we assumed that the N/C ratio is $2 \times$ solar, with an uncertainty of 0.20 dex, in normal main-sequence O stars; we assumed that N/C ratio is $4 \times$ solar, with an

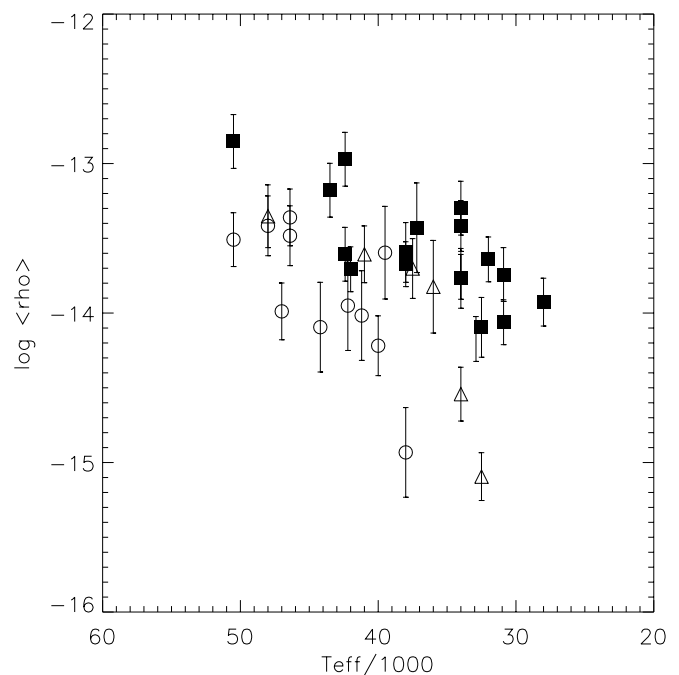


FIG. 2.—Distribution of the program stars in the T_{eff} vs. $\log \langle \rho \rangle$ diagram. The stars occupy approximately a triangular region, with the lower limit corresponding to the main sequence. Note that T_{eff} and $\langle \rho \rangle$ are not correlated. Symbols are the same as in Fig. 1.

uncertainty of 0.30 dex, in the moderately N-deficient stars ζ Ori and ϵ Ori; and finally, we assumed that the N/C ratio is $11 \times$ solar, with an uncertainty of 0.40 dex, for all other stars. The adopted solar abundances are: $\log(N/H) = -4.16$, $\log(C/H) = -3.48$, $\log(\text{Si}/H) = -4.40$, $N/C = 0.21$, and $\text{He}/H = 0.10$. The sum $N + C$ is constant compared to $H + \text{He}$, i.e., $(C + N)/(H + \text{He}) = 3.6 \times 10^{-4}$, since C is converted into N by the CN cycle.

The resulting abundances of C and N, with their uncertainties, are:

For O IV and O V stars: $\log(N/H_0)_* = -3.93 \pm 0.14$ and $\log(C/H_0)_* = -3.55 \pm 0.06$.

For ζ Ori and ϵ Ori: $\log(N/H_0)_* = -3.74 \pm 0.16$ and $\log(C/H_0)_* = -3.66 \pm 0.14$.

For other O stars: $\log(N/H_0)_* = -3.56 \pm 0.13$ and $\log(C/H_0)_* = -3.92 \pm 0.27$.

In the above values, H_0 is the *initial* H abundance. Note that the uncertainties in the abundances are smaller than the uncertainties in the N/C ratio, since the $N + C$ abundance is fixed. We adopted the solar Si abundances for all stars.

For the abundance of helium, we adopted the values derived for the individual stars in the studies of Voels et al. (1989), Herrero et al. (1992), Pauldrach et al. (1994), and Puls et al. (1995). For those stars not included in one of these studies, we adopted the following He/H ratios by number: 0.08 for stars of luminosity classes IV and V, 0.12 for classes II and III, and 0.15 for class I.

3. OPTICAL DEPTHS AND IONIZATION FRACTIONS

3.1. The Definition of the Mean Ionization Fractions

P Cygni profiles formed in stellar winds depend on only two functions: the velocity law, $v(r)$, and the Sobolev optical depth, $\tau(v)$. If the wind has chaotic motions, the profile also depends on the resulting velocity dispersion, usually called the “turbulent” velocity, although the motions are not due to real turbulence. The line fits of GL and Haser (1995) show that the wind has a chaotic velocity component due to the presence of shocks. This effect was taken into account by adopting a velocity dispersion in the wind. In the analysis of GL, the velocity dispersion was assumed to be constant throughout the wind, with typical values of about $100\text{--}300 \text{ km s}^{-1}$. Haser assumed a variable velocity dispersion that increased with the wind velocity, from about 50 km s^{-1} at the bottom of the wind to about $100\text{--}300 \text{ km s}^{-1}$ at large distances. The difference between the adopted turbulent velocities has only a small effect on the ionization fractions derived in this study (see § 3.2).

The velocity law of radiation-driven winds can be characterized by a β -law:

$$w(x) = w_0 + (1 - w_0) \left(1 - \frac{1}{x}\right)^\beta, \quad (2)$$

where w and x are the normalized velocity, $w \equiv v/v_\infty$, and distance $x \equiv r/R_*$ (Pauldrach et al. 1986; GL). The value of w_0 is small, usually on the order of 0.01 for O stars. Its exact value is not important for this study. Haser adopted a slightly different velocity law,

$$w(x) = \left(1 - \frac{b}{x}\right)^\beta, \quad (3)$$

with $b = 1 - w_0^{1/\beta}$ and $w_0 = 0.01$. This formula gives almost the same velocity structure for $w(x) > w_0$ as equation (2),

but it can be integrated analytically in the expression for the column density.

The radial Sobolev optical depth is

$$\tau(w) \equiv \frac{\pi e^2}{mc} f_{lu} \lambda_0 \frac{R_*}{v_\infty} n_l \left(1 - \frac{n_u g_l}{n_l g_u}\right) \left(\frac{dw}{dx}\right)^{-1}, \quad (4)$$

where f_{lu} is the oscillator strength, λ_0 is the rest wavelength, g is the statistical weight, and n is the ion number density of the lower (subscript l) and upper (subscript u) levels of the transition. For resonance lines and lines from low excited levels, we can ignore the factor $(n_u g_l/n_l g_u)$.

The number density of ions in the lower level of the transition can be written as

$$\begin{aligned} n_l(x) &= \frac{n_i(x)}{n_i(x)} \frac{n_i(x)}{n_E(x)} \frac{n_E}{n_H} \frac{n_H}{\rho} \\ &\equiv q_{\text{exc}}(x) q_i(x) A_E \frac{n_H}{\rho} \frac{\dot{M}}{4\pi R_*^2 v_\infty} \frac{1}{x^2 w}, \end{aligned} \quad (5)$$

where $n_i(x)$ is the number density of the observed ion, $n_E(x)$ is the number density of the observed element, and $n_H(x)$ is the number density of hydrogen. In the second part of the equation we have used the continuity equation $\dot{M} = 4\pi r^2 v \rho$, together with the definitions of the excitation fraction, $q_{\text{exc}} \equiv n_l/n_i$, the ionization fraction, $q_i \equiv n_i/n_E$, and the element abundance, $A_E \equiv n_E/n_H$. We can assume that $q_{\text{exc}} = 1$ for resonance lines, since the vast majority of the ions in a stellar wind will be in their ground state. The ratio $n_H/\rho = 4.420 \times 10^{23} \text{ g}^{-1}$ for Population I composition.

Combining equations (4) and (5), we can express the Sobolev optical depth as

$$\begin{aligned} \tau(w) &= \frac{1}{4\pi} \frac{\pi e^2}{mc} f_{lu} \lambda_0 A_E \frac{n_H}{\rho} \frac{\dot{M}}{R_* v_\infty^2} q_i(x) q_{\text{exc}}(x) \\ &\quad \times \frac{1}{x^2 w} \frac{dx}{dw}. \end{aligned} \quad (6)$$

This equation shows that the ionization and excitation fractions in a stellar wind can be derived from the values of $\tau(w)$, which can be found from line-profile fitting if the mass-loss rate, the terminal velocity, and the velocity law are known.

We define the *mean ionization and excitation fraction* over the distance in the wind where $v(r)$ varies between $w_a v_\infty$ and $w_b v_\infty$ as the ratio between the ion and element column densities,

$$\begin{aligned} \langle q \rangle &\equiv \frac{N_i}{N_E} \equiv \frac{N_i}{A_E N_H} \\ &\equiv \frac{\int_{x(w_a)}^{x(w_b)} n_i(x) dx}{\int_{x(w_a)}^{x(w_b)} n_E(x) dx}. \end{aligned} \quad (7)$$

Our definition of $\langle q \rangle$ is the density mean of q_i for resonance lines (which have $q_{\text{exc}} = 1$), and the density mean of $q_{\text{exc}} q_i$ for lines from excited levels. From equations (4), (5), and (6), we see that this implies

$$\langle q \rangle = 4\pi \frac{mc}{\pi e^2} \frac{1}{f_{lu} \lambda_0 A_E} \frac{\rho}{n_H} \frac{R_* v_\infty^2}{\dot{M}}$$

$$\times \frac{\int_{w_a}^{w_b} \tau(w) dw}{\int_{w_a}^{w_b} (x^2 w)^{-1} (dx/dw) dw}. \quad (8)$$

The integrated Sobolev optical depth between w_a and w_b of a line of ion i is

$$T_i \equiv \int_{w_a}^{w_b} \tau(w) dw, \quad (9)$$

which is the integral that enters into the expression for $\langle q \rangle$ in equation (8). We used $w_a = 0.2$ and $w_b = 0.8$ for the line fits from GL, and $w_a = 0.2$ and $w_b = 1.0$ for the line fits from Haser (1995). The difference in the value of $\langle q \rangle$ due to the difference in these ranges is less than about 25%. This is much smaller than the uncertainty in $\langle q \rangle$ due to other factors.

For typical values of $f_{ul} \simeq 0.1$, $\lambda_0 \simeq 1000 \text{ \AA}$, $R_* \simeq 10 R_\odot$, $v_\infty \simeq 2000 \text{ km s}^{-1}$, $\dot{M} \simeq 10^{-5} M_\odot \text{ yr}^{-1}$, and $T_i \simeq 1$, we find $A_E \langle q \rangle \simeq 3 \times 10^{-8}$. This corroborates our earlier statement that only resonance lines from trace elements or from trace ions of abundant elements will produce unsaturated P Cygni profiles.

We will derive the values of $\langle q(\text{N v}) \rangle$, $\langle q(\text{C iv}) \rangle$, and $\langle q(\text{Si iv}) \rangle$ from the resonance lines of these ions, $\langle q(\text{C III}^*) \rangle$ from the subordinate line at 1176 \AA, and $\langle q(\text{N IV}^*) \rangle$ from the subordinate line at 1718 \AA. The adopted atomic data are given in Table 2.

3.2. The Optical Depths of the P Cygni Profiles

The P Cygni profiles of all program stars were studied by Haser (1995), and most of them are also studied by GL. In both papers the observed line profiles are studied with the SEI method (Hamann 1981; Lamers et al. 1987). Haser studied the UV lines of N v, C iv, Si iv and N IV* observed with the IUE satellite. GL studied the same lines, and also included the C III* line at 1176 \AA. In all cases, both authors found good agreement between the observed and theoretical line profiles. The column densities derived by the two groups agree very well with one another (see Haser 1995).

The line fits by Haser (1995) are more accurate than those by GL, because Haser adopted a better representation of the velocity dispersion in the wind (see below), which results in theoretical profiles that agree better with the observed profiles. Therefore, we adopted the column densities of C iv, N v, Si iv and N IV* from Haser, and those of C III* from GL.

GL expressed the Sobolev optical depth of the lines as a mathematical function of the type

$$\tau(w) = \left\{ \frac{T_i}{I} \right\} \left\{ \frac{w}{w_1} \right\}^{\alpha_1} \left\{ 1 - \left(\frac{w}{w_1} \right)^{1/\beta} \right\}^{\alpha_2} \quad (10)$$

for $w \leq w_1$, and

$$\tau(w) = 0 \quad (11)$$

for $w > w_1$, where w is the normalized velocity $w = v(r)/v_\infty$. The normalization factor I is

$$I = \int_{w_0}^{w_1} \left\{ \frac{w}{w_1} \right\}^{\alpha_1} \left\{ 1 - \left(\frac{w}{w_1} \right)^{1/\beta} \right\}^{\alpha_2} dw. \quad (12)$$

The normalization factor I assures that T_i is the integrated Sobolev optical depth, which is directly related to the column density N_i of the observed ion in the wind via

$$T_i = \frac{\pi e^2}{mc} \frac{f_{lu} \lambda_0}{v_\infty} N_i. \quad (13)$$

The free fitting parameters are T_i , α_1 , and α_2 . The parameter w_1 describes the extent of the violet absorption in terms of v_∞ . A value of $w_1 = 1$ always holds for resonance lines, but w_1 can be smaller for lines from excited levels when the violet absorption wings do not reach v_∞ . The choice of equation (10) for $\tau(w)$ is based on the following consideration. If the ionization in the wind varies with distance or with velocity in the wind as a power law of the type $q_i \propto x^{-s} w^{-t}$, then τ will vary as $\tau \propto w^{\alpha_1} (1 - w^{1/\beta})^{\alpha_2}$, with $\alpha_1 = \beta^{-1} - 2 - t$ and $\alpha_2 = +s$. The adopted simple function for τ gives very good fits to the observed P Cygni profiles and violet absorption wings.

Haser (1995) adopted an optical depth law that varies as a combination of two power laws of the velocity:

$$\begin{aligned} \tau(v) &\propto v^{\alpha_i} & \text{for } v_{\min} < v < v_{i0}, \\ \tau(v) &\propto v^{\alpha_o} & \text{for } v_{i0} < v < v_\infty, \end{aligned} \quad (14)$$

where α_i , α_o , and v_{i0} , together with the normalization constant, are the fit parameters.

We want to stress that the choice of the formulae for representing $\tau(w)$ is not unique, and other mathematical expressions might also give good fits to the profiles. However, this would not change the results. This is because the profile of an unsaturated line, for a given velocity law and velocity dispersion, depends *only on* $\tau(w)$ in the relevant velocity range. *Therefore, a good fit to the observed line profiles implies that the numerical values of $\tau(w)$ must be close to the correct value, whichever mathematical representation of $\tau(w)$ is chosen.*

The line fits resulted in the determination of the Sobolev optical depth $\tau(w)$ for each line in each star. Many line profiles studied by GL and Haser (1995) are saturated or nearly saturated, in particular the C iv and the N v lines. In those cases, we have assigned lower limits to the values of the optical depths. For saturated lines, we adopted a lower limit of $T_i > 4$ for the blue components of the C iv and N v lines, and $T_i > 2$ for the red components. This is because the two components of these lines overlap in the spectra of O stars. For saturated Si iv lines, we adopted a lower limit of $T_i > 8$ and $T_i > 4$ for the blue and red components, respectively. This is because the two components are usually separated in the spectra of O stars, so the red component may be unsaturated even if the blue component is saturated. These limits agree with the upper limits of the column densities derived from the line fits by Haser (1995).

TABLE 2
ATOMIC DATA

Ion	λ_0	f_{lu}	g_l	g_u	χ_{exc} (eV)
C iv	1548.19	0.194	2	4	0.00
	1550.76	0.097	2	2	
N v	1238.81	0.152	2	4	0.00
	1242.77	0.078	2	2	
Si iv	1393.76	0.528	2	4	0.00
	1402.77	0.262	2	2	
N iv	1718.55	0.179	1	3	16.21
C III	1175.66 ^a	0.257	1	9	6.50

^a C III 1175 is a composite of six lines.

When a line does not show extended violet wings or a P Cygni profile, an upper limit of the optical depth T_i was assigned. The upper limit is $T_i < 0.2$ for all the lines, except for the N IV* line, which is in a clean spectral region without strong blends. For a N IV* profile with no wind component, we adopted $T_i < 0.1$. We have carefully checked the accuracy of the line fits to assign an uncertainty to T_i . Observed lines with a low S/N ratio have a larger uncertainty. These are typically the C III* lines (and for some stars also the N V lines), because the S/N ratio of IUE spectra at $\lambda < 1200 \text{ \AA}$ is low.

3.3. The Empirical Ionization Fractions

The optical depths are converted into column densities using equation (13). The mean ionization and excitation fractions are derived from the optical depths by means of equation (8). Haser (1995) has listed the column densities in the wind derived from the lines of C IV, N V, Si IV and N IV* in the interval $0.2v_\infty$ to v_∞ . GL have listed the values of their line fits, α_1 and α_2 , and T , from which we derived the values of the column densities and $\log \langle q \rangle$ in the distance range where v varies between $0.2v_\infty$ to $0.8v_\infty$. The resulting values of $\log \langle q \rangle$ are listed in Table 3. Note that the values of $\langle q(\text{C IV}) \rangle$, $\langle q(\text{N V}) \rangle$, $\langle q(\text{Si IV}) \rangle$, and $\langle q(\text{N IV}^*) \rangle$ refer to the distance interval $[0.2v_\infty, v_\infty]$, whereas $\langle q(\text{C III}^*) \rangle$ refers to $[0.2v_\infty, 0.8v_\infty]$.

The uncertainty in $\log \langle q \rangle$ mainly depends on the uncertainty in \dot{M} and v_∞ , the uncertainty in the abundance, and the uncertainty in the optical depth of the line. We adopted

$$\Delta \log \langle q \rangle = \sqrt{(\Delta \log \dot{M})^2 + (\Delta \log A_E)^2 + (\Delta \log N_i)^2}. \quad (15)$$

The very small uncertainty in v_∞ can be ignored compared to the uncertainties in the other parameters. The values of $\Delta \log N_i$ are typically 0.1 for a good line fit of an unsaturated line and 0.3 for a slightly worse line fit when a line is partly saturated. The uncertainties in A_E and in $\log \dot{M}$ are given in § 2.3 and in Table 1, respectively. The uncertainties in $\log \langle q \rangle$ are typically 0.3 to 0.4 dex for unsaturated lines. The uncertainties are listed in Table 3. In the case of upper or lower limits, we took the uncertainties into account and adopted the conservative values of $\log \langle q \rangle - \Delta \log \langle q \rangle$ for lower limits and $\log \langle q \rangle + \Delta \log \langle q \rangle$ for upper limits.

3.4. Comparison with Other Determinations

Howarth & Prinja (1989) derived the ionizations for 203 O stars from line fits with the Sobolev method, which is much less accurate than the SEI method used by GL and Haser (1995). Howarth & Prinja adopted solar abundances and derived mean empirical ionization fractions from their total sample: $\langle q(\text{C IV}) \rangle = -2.86 \pm 0.44$, $\langle q(\text{N V}) \rangle = -2.57 \pm 0.61$, and $\langle q(\text{Si IV}) \rangle = -3.56 \pm 1.07$.

TABLE 3
MEAN IONIZATION FRACTIONS

HD	$\log \langle q(\text{C IV}) \rangle$	$\log \langle q(\text{N V}) \rangle$	$\log \langle q(\text{Si IV}) \rangle$	$\log \langle q(\text{N IV}^*) \rangle$	$\log \langle q(\text{C III}^*) \rangle$
14947	> -3.35	...	-3.14 ± 0.27	-4.10 ± 0.30	...
15558	> -3.07	...	-3.63 ± 0.29	-4.24 ± 0.32	...
15570	> -2.86	...	< -3.56
15629	> -2.45	-1.87 ± 0.31	< -2.89	-3.52 ± 0.31	...
36486	-2.41 ± 0.37	-3.31 ± 0.28	-2.64 ± 0.25
36861	-2.46 ± 0.46	-2.70 ± 0.39	< -3.05	< -3.79	-3.24 ± 0.51
37043	-2.07 ± 0.38	-2.53 ± 0.30	< -2.60	< -3.33	-3.10 ± 0.44
37128	> -3.24	-3.50 ± 0.30	-2.36 ± 0.26	< -4.33	-2.91 ± 0.37
37742	-2.86 ± 0.29	-3.30 ± 0.30	-2.51 ± 0.25	< -3.94	> -2.84
46223	> -3.06	> -2.52	< -3.50	-3.81 ± 0.31	...
47839	-3.19 ± 0.37	-2.86 ± 0.39	< -3.16	< -3.52	...
57061	-2.62 ± 0.37	-3.72 ± 0.28	-3.22 ± 0.25
66811	> -2.77	> -2.82	-2.98 ± 0.25	-3.12 ± 0.28	-3.26 ± 0.43
93129	-3.37 ± 0.38	-3.26 ± 0.30	< -4.15	-4.42 ± 0.30	...
93204	> -2.37	-1.49 ± 0.39	< -2.60	...	< -2.88
93250	-3.29 ± 0.28	-2.60 ± 0.30	< -3.54	-3.89 ± 0.30	< -3.82
101190	-2.65 ± 0.37	-1.65 ± 0.39	< -2.90	-3.08 ± 0.39	< -3.18
101413	-1.98 ± 0.37	-1.62 ± 0.39	< -1.75	< -2.11	< -2.03
101436	-2.44 ± 0.37	-2.11 ± 0.39	< -2.80	< -3.16	< -3.07
149038	> -3.03	-3.44 ± 0.30	-2.65 ± 0.27	< -4.46	-3.37 ± 0.44
149404	> -3.20	> -3.24	> -2.66
149757	-1.80 ± 0.37	-2.51 ± 0.29
151804	> -3.49	> -3.53	> -2.95	...	> -3.49
163758	> -3.25	> -3.34	> -2.76	-3.92 ± 0.38	-3.05 ± 0.50
164794	> -3.09	> -2.53	< -3.51	-3.76 ± 0.32	...
188001	> -3.41	> -3.47	> -2.89	< -4.85	-3.38 ± 0.44
190429	> -3.54	> -3.60	-3.86 ± 0.27	-4.06 ± 0.30	...
190864	> -2.67	-2.59 ± 0.30	-3.27 ± 0.28	-4.19 ± 0.30	< -3.13
193514	> -3.07	...	-2.92 ± 0.29	-4.45 ± 0.31	...
203064	> -2.58	-2.54 ± 0.31	-2.78 ± 0.29
207198	> -2.79	-3.36 ± 0.31	-3.11 ± 0.29
209975	> -2.54	-2.97 ± 0.31	-2.40 ± 0.29	< -3.93	...
210839	> -2.75	> -2.80	-2.45 ± 0.25	-3.65 ± 0.28	-3.27 ± 0.43
217086	-1.73 ± 0.29	-1.76 ± 0.32
303308	> -2.94	> -2.39	< -3.36	-3.76 ± 0.32	...

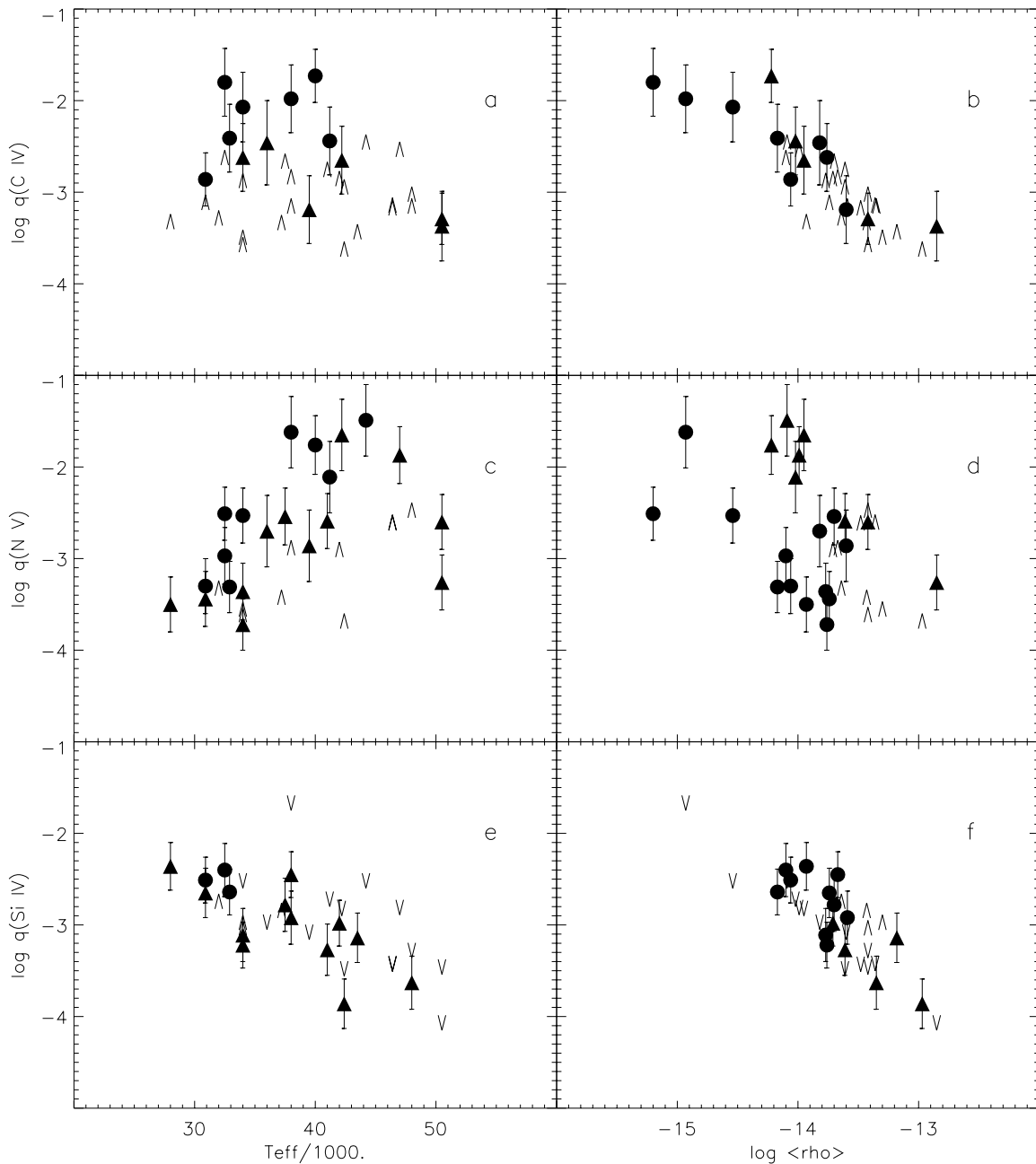


FIG. 3.—Mean ionization fractions, $\log \langle q \rangle$, as a function of T_{eff} (left panels) or $\log \langle \rho \rangle$ (right panels) for $\langle q(\text{C IV}) \rangle$, $\langle q(\text{N V}) \rangle$, and $\langle q(\text{Si IV}) \rangle$. Left panels: filled circles show stars with $\langle \rho \rangle \leq 10^{-14}$, triangles those with $\langle \rho \rangle > 10^{-14}$ g cm $^{-3}$. Right panels: filled circles show stars with $T_{\text{eff}} < 40,000$ K, triangles those with $T_{\text{eff}} \geq 40,000$ K. Upper and lower limits are indicated by arrows. For most ions, $\log \langle q \rangle$ depends on a combination of both $\langle \rho \rangle$ and T_{eff} . Typical uncertainties in the stellar parameters are $\Delta \log \langle \rho \rangle \approx 0.3$ and $\Delta T_{\text{eff}} \approx 3000$ K for early O stars, 2000 K for late O stars (see Table 1).

The mean values derived from our sample are $\langle q(\text{C IV}) \rangle = -2.53 \pm 0.54$, $\langle q(\text{N V}) \rangle = -2.65 \pm 0.69$, and $\langle q(\text{Si IV}) \rangle = -2.93 \pm 0.45$. Although these mean values agree with one another within the uncertainties, the comparison is not very meaningful, since, as we show below, the ionization fractions vary strongly from star to star because they depend on both T_{eff} and on the mean density in the wind.

4. THE DEPENDENCE OF THE IONIZATION FRACTIONS ON THE STELLAR PARAMETERS

The purpose of this paper is to derive relations between stellar parameters and mean ionization fractions. Figures 3 and 4 show the variations of $\log \langle q \rangle$ with T_{eff} and with

$\langle \rho \rangle$. These figures are not expected to show simple trends, because the ionization fractions may depend on both parameters T_{eff} and $\langle \rho \rangle$. To indicate this two-dimensional dependence, in Figures 3 and 4 we use filled circles for the stars with $\log \langle \rho \rangle < -14.0$ and triangles for stars with $\log \langle \rho \rangle > -14.0$ in the plots of $\log \langle q \rangle$ versus T_{eff} . Similarly, we use filled circles for the stars with $T_{\text{eff}} < 40,000$ in the plots of $\log \langle q \rangle$ versus $\langle \rho \rangle$ and triangles for stars with $T_{\text{eff}} > 40,000$. Upper and lower limits are indicated by arrows.

4.1. Discussion of the Relations

1. C IV (Figs. 3a and 3b).—The C IV profiles in many O stars are saturated. The stars with actual $\langle q(\text{C IV}) \rangle$ values

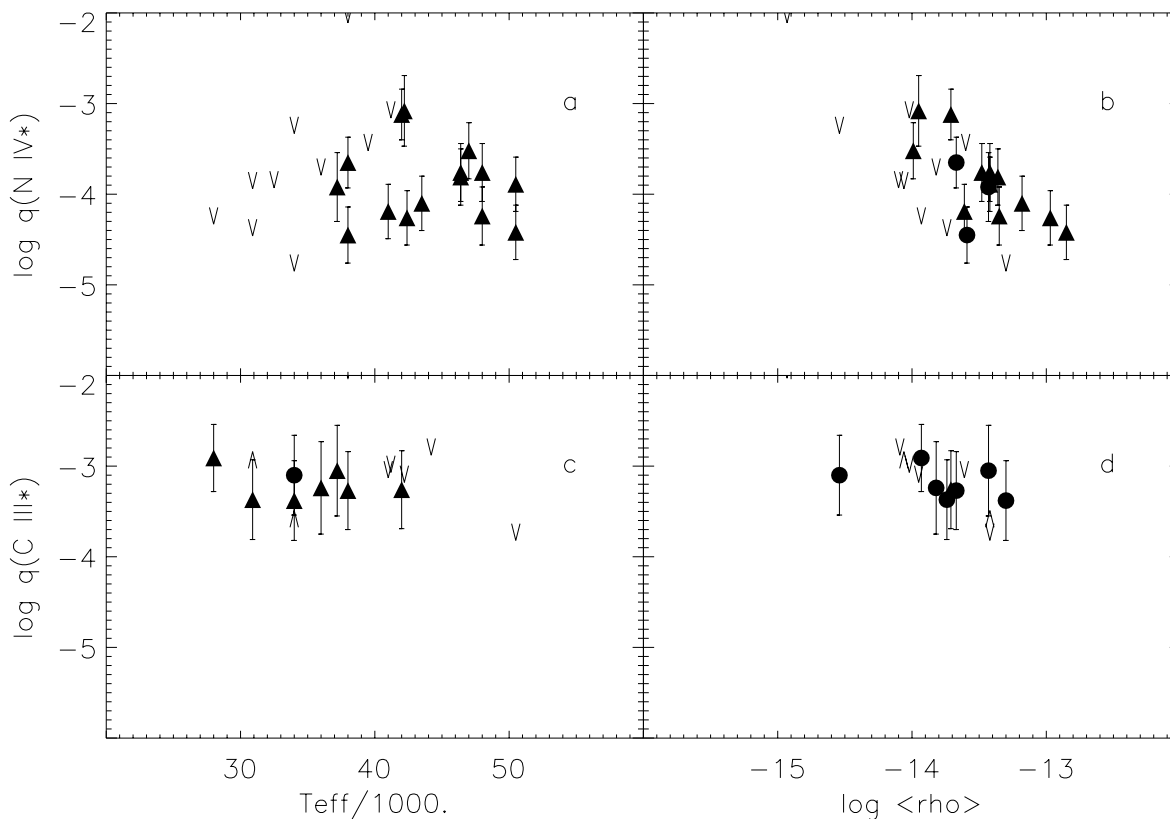


FIG. 4.—Mean ionization fractions as a function of $\log \langle q \rangle$ and T_{eff} (left panels) or $\log \langle \rho \rangle$ (right panels) for $\langle q(\text{N IV}^*) \rangle$ and $\langle q(\text{C III}^*) \rangle$. Symbols are as in Fig. 3.

(as opposed to limits only) have ionization fractions between -1.7 and -3.5 . The stars with a lower limit might have higher values. Figure 3b suggests that the mean ionization fraction decreases with $\langle \rho \rangle$. We will argue in § 4.2 that this may be due to a selection effect.

2. N v (Figs. 3c and 3d).—The N v profiles in the spectra of many O stars are saturated. Figure 3c shows the relation between $\langle q(\text{N v}) \rangle$ and T_{eff} . There is clearly a correlation in the temperature region between $T_{\text{eff}} = 28,000$ and $42,000$ K, where the ionization fraction increases with temperature from -3.7 dex near $T_{\text{eff}} = 28,000$ K to about -1.7 dex at $42,000$ K. The distribution of filled circles and triangles shows that at any temperature, stars with a higher wind density have a lower ionization fraction of N v. Figure 3d shows the variation of $\langle q(\text{N v}) \rangle$ with $\log \langle \rho \rangle$. There is no clear relation between $\langle q(\text{N v}) \rangle$ and $\langle \rho \rangle$, because the strong dependence of $\langle q(\text{N v}) \rangle$ on T_{eff} dominates the relations: circles are systematically lower than triangles.

3. Si iv (Figs. 3e and 3f).—The Si iv lines are saturated in many O stars and absent in others. Figure 3e shows that the ionization fraction of Si iv decreases toward higher temperatures, from about -2.4 dex near $30,000$ K to -4.0 dex near $50,000$ K. Figure 3f suggests that the ionization fraction of Si iv decreases with density. We will show in § 4.2 that this is likely due to a selection effect.

4. N iv* (Figs. 4a and 4b).—The N iv* lines have profiles with extended violet absorption wings in early O stars. The spectra of late O stars do not show these wind features. Therefore, we find only upper limits for stars with $T_{\text{eff}} < 40,000$ K. Figure 4b suggests an inverse density dependence of the ionization fraction.

5. C III* (Figs. 4c and 4d).—The spectra of late O stars show wind features in the C III* line, whereas this line is not present in the spectra of early O stars. Unfortunately, the line is located in a part of the spectrum that is usually noisy in IUE observations. Still, Figure 4c shows that the mean ionization and excitation fraction is about constant at -3.2 dex in the range between $28,000$ and $38,000$ K. The C III* lines in hotter stars usually do not show wind features, with only ζ Pup (O4 If) at $T_{\text{eff}} = 42,000$ K as an exception.

4.2. On the $\langle \rho \rangle^{-1}$ Dependence of $\langle q \rangle$

The data plotted in Figures 3 and 4 suggest that the mean ionization fractions of C iv and Si iv depend on the mean density of the wind as $\langle q \rangle \propto \langle \rho \rangle^{-1} \propto \dot{M}^{-1}$. This is surprising, because it is contrary to the expected dependence. For instance, for Si iv, we expect that $\langle q(\text{Si iv}) \rangle \propto \langle \rho \rangle^{+1}$, because Si v is the dominant ionization stage of Si in the winds of O stars, and the recombination rate is proportional to ρ^{+1} (see Haser 1995). In general, if the ionization equilibrium is determined by recombination and photoionization in a wind that is optically thin for the ionizing continuum, we expect the ionization fraction of an ion to depend on $\langle \rho \rangle^{d-i}$, if d indicates the dominant ionization stage (e.g., $d = 4$ for Si v) and i is the observed ionization stage (e.g., $i = 3$ for Si iv). We expect C v to be the dominant stage of ionization for C, so intuitively we predicted that $\langle q(\text{C iv}) \rangle \sim \langle \rho \rangle^{+1}$, contrary to the empirical relations.

A simple analysis shows that the observed $\langle q \rangle \propto \langle \rho \rangle^{-1}$ relations are due to an observational selection effect if many stars have either saturated lines or lines that are too faint. This selection effect is caused by the fact that we can only

determine accurate values of $\langle q \rangle$ from P Cygni profiles that are neither saturated nor too faint. This sets limits to the Sobolev optical depth T_i in the range of about $0.1 < T_i < 4$ (see § 3.2). The optical depth is proportional to

$$T_i \propto \frac{N_i}{v_\infty} \propto \frac{\dot{M}}{R_* v_\infty^2} \langle q \rangle \quad (16)$$

(eq. [13]), so the mean ionization fraction is proportional to

$$\langle q \rangle \sim \frac{T_i R_* v_\infty^2}{\dot{M}} \sim \frac{T_i v_\infty}{R_*} \frac{1}{\langle \rho \rangle}. \quad (17)$$

We see that $\langle q \rangle \propto \langle \rho \rangle^{-1}$. The values of T_i for unsaturated P Cygni profiles vary by about a factor of 40. The values of v_∞/R_* vary by a factor of about 7 for our sample of stars, but the values of $\langle \rho \rangle$ vary by a factor of 200. Therefore, the largest variation of $\langle q \rangle$ is due to the variation of $\langle \rho \rangle$ in our sample of stars. In other words, if the true ionization fractions were completely uncorrelated with any of the stellar parameters, we would only be able to derive accurate values of $\langle q \rangle$ for those stars that cover a strip in the $\langle q \rangle, \langle \rho \rangle$ diagram. Figure 3 indeed shows evidence for this selection effect in C IV, and possibly also in Si IV.

5. EMPIRICAL RELATIONS FOR THE IONIZATION FRACTIONS

Haser (1995) has shown that the mean ionization fraction of Si IV in the winds of O stars can be expressed in terms of a modified nebular approximation, with a radiation temperature that is a simple function of T_{eff} . In this section we attempt to describe the ionization fractions of the observed ions in similar terms.

In the modified nebular approximation, where the ionization equilibrium is due to photoionization and recombination, the ionization ratio between two successive stages of ionization is given by

$$\frac{n_{i+1}}{n_i} \simeq \frac{2U_{i+1}}{U_i} \left(\frac{2\pi m_e k}{h^2} \right)^{3/2} \frac{W}{n_e} \sqrt{T_e} T_{\text{rad}} e^{-\chi/kT_{\text{rad}}} \quad (18)$$

(Mihalas 1970), where U is the partition function, T_e is the electron temperature, and χ is the ionization energy of stage i . T_{rad} is the radiation temperature (more correctly the brightness temperature) of the photosphere in the wavelength range of the ionizing continuum, i.e., at $\lambda(\text{\AA}) < 11605/\chi(\text{eV})$. The geometrical dilution factor is $W = 0.5[1 - (1 - 1/x^2)^{1/2}]$. Equation (18) is strictly valid if the wind is optically thin for the ionizing continuum radiation. However, we can also apply it if the wind is not optically thin for the ionizing radiation to derive an *empirical* radiation temperature. In that case, the value of T_{rad} does not describe the real brightness temperature of the photosphere in the ionizing continuum, but it gives a convenient parameter to describe the ionization fraction.

If we assume that one of the stages, $i+1$ or i , is the dominant stage of ionization, then $n_{i+1} = n_E$ or $n_i = n_E$, where n_E is the number density of atoms of the element E . In that case, we can use equation (18) to describe the number density of the observed ions. The column densities of the ions can then be found by integrating n along the line of sight to the star. Comparing the column densities N_E with the values of N_i derived from the UV lines of the five ions results in a determination of the radiation temperature for each observed ion in each star. In this analysis, we assume

an electron temperature of $T_e = 0.8T_{\text{eff}}$. We also assume that H is fully ionized, He is singly ionized in the winds of stars with $T_{\text{eff}} < 30,000$ K, 1.5 times ionized if $30,000 \text{ K} \leq T_{\text{eff}} < 35,000$ K, and twice ionized if $T_{\text{eff}} \geq 35,000$ K (Lamers & Leitherer 1993, based on non-LTE calculations by de Koter).

5.1. The Ionization of Si IV

The mean ionization fractions discussed in § 4 show that Si IV is not the dominant stage of ionization in the winds of O stars. The ionization potential of Si V is very high, 166.8 eV, so there will be very little Si VI. This leaves Si V as the dominant stage of ionization of Si. The ionization potential of Si IV is 45.1 eV, so the ionizing radiation is at $\lambda < 275 \text{ \AA}$. This is in the He I continuum, for which the wind is optically thin, so equation (18) is expected to provide a good description of the ionization ratio $n(\text{Si IV})/n(\text{Si V})$ (Haser 1995). Combining this equation with the mass continuity equation gives an expression for the column density $N(\text{Si IV})$:

$$N(\text{Si IV}) = 3.09 \times 10^{-9} \frac{n_e}{\rho} \frac{n(\text{Si})}{\rho} \frac{\dot{M}^2}{R_*^3 v_\infty^2} \frac{1}{\sqrt{T_e}} \frac{I_1}{f_{\text{rad}}(\text{Si IV})}, \quad (19)$$

with \dot{M} in $M_\odot \text{ yr}^{-1}$, v_∞ in km s^{-1} , R_* in R_\odot , and

$$f_{\text{rad}}(\text{Si IV}) = T_{\text{rad}}(\text{Si IV}) e^{-5.234 \times 10^5 / T_{\text{rad}}(\text{Si IV})}. \quad (20)$$

We see that the expected column density of Si IV depends on $(\dot{M}/v_\infty)^2 \propto \rho^2$. This is because the ionization fraction $q(\text{Si IV})$ is proportional to ρ if Si V is the dominant ionization stage (see § 4.2) and the ion density is $n(\text{Si IV}) \propto \rho q(\text{Si IV})$.

The integration over the column density between $x(w=0.2)$ and $x = \infty$ gives an integral

$$I_1 = \int_{x(w=0.2)}^{\infty} \frac{dx}{W x^4 w^2}. \quad (21)$$

This integral depends on the value of β that describes the velocity law: $I_1 = 12.7, 13.4,$ and 14.2 for $\beta = 0.7, 0.8,$ and 1.0 , respectively.

The comparison between the observed and predicted column density of Si IV yields the values of $T_{\text{rad}}(\text{Si IV})$ for each star. These values are plotted in terms of $T_{\text{rad}}/T_{\text{eff}}$ versus T_{eff} in Figure 5a. This ratio shows an almost linear correlation with T_{eff} , as was already found by Haser (1995). A quadratic least-square fit gives the relation

$$\frac{T_{\text{rad}}(\text{Si IV})}{T_{\text{eff}}} = 1.878 - 1.892 \left(\frac{T_{\text{eff}}}{40,000} \right) + 0.748 \left(\frac{T_{\text{eff}}}{40,000} \right)^2. \quad (22)$$

This relation is valid in the temperature range of $27,000 \text{ K} < T_{\text{eff}} < 48,000 \text{ K}$. The upper and lower limits agree with this relation, within their accuracy. The resulting values of $f_{\text{rad}}(\text{Si IV})$ are compared with the empirical ones in Figure 5b. The ratio has a scatter of $\sigma = 0.22$ dex. Since $\dot{M} \propto (f_{\text{rad}})^{1/2}$, the scatter in the mass-loss rates derived from the Si IV lines is expected to be about 0.11 dex, if the stellar parameters are accurately known.

Our analysis shows that Si IV is not the dominant stage of ionization in the winds of O stars. The trends of $\langle q(\text{Si IV}) \rangle$ suggest that the ionization fraction of Si IV reaches its maximum at $T_{\text{eff}} < 30,000 \text{ K}$. This agrees with the strength

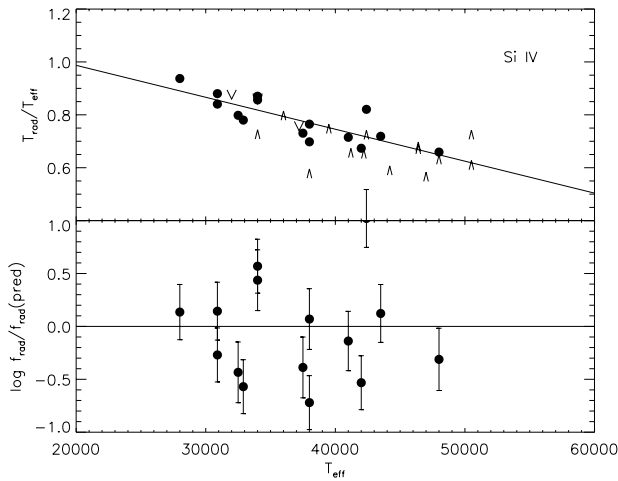


FIG. 5.—*Top*: ratio $T_{\text{rad}}/T_{\text{eff}}$ of Si IV as a function of T_{eff} . The solid line shows the best-fit quadratic relation. *Bottom*: ratio between the empirical value of f_{rad} and the one predicted by the best-fit relation of the top figure.

of the Si IV lines in the atlas of UV P Cygni profiles by Snow et al. (1994) and with the study of the P Cygni profiles of the B supergiants by Haser (1995). They show that the Si IV wind lines are very strong and saturated for supergiants of spectral types as late as B2 with $T_{\text{eff}} \approx 20,000$ K.

5.2. The Ionization of C IV

The variation of $\langle q(\text{C IV}) \rangle$ with T_{eff} and $\langle \rho \rangle$, shown in Figures 3a and 3b, has many lower limits. This is especially true for winds with mean densities larger than 10^{-14} g cm $^{-3}$. We expect that C IV is the dominant ionization stage in the winds of stars with $30,000 \text{ K} < T_{\text{eff}} < 37,000 \text{ K}$ (de Koter 1993). Therefore, many of the lower limits of the ionization fraction of C IV may indicate $\langle q(\text{C IV}) \rangle \approx 1$. So, we cannot derive an empirical relation between the ionization fraction of C IV and the stellar parameters for stars with high wind densities. We have tried to express the ionization fractions of the stars with unsaturated C IV lines in terms of a radiation temperature similar to equation (20). However, the resulting values of T_{rad} (C IV) do not simply scale with T_{eff} . This is because the ionization fraction of C IV depends on the ratio between $n(\text{C V})/n(\text{C IV})$ and hence on the ionizing radiation in the He II continuum. The radiation temperature of the He II continuum does not simply scale with T_{eff} , because it depends sensitively on the optical depth of the wind. Winds with $\log \langle \rho \rangle < -14$ do not show saturated C IV lines. These stars have $\langle q(\text{C IV}) \rangle$ values of

$$\log \langle q(\text{C IV}) \rangle \approx -2.00 \pm 0.27 \quad (23)$$

for stars with $32,000 \text{ K} \leq T_{\text{eff}} < 40,000 \text{ K}$ and $\log \langle \rho \rangle \leq -14.0$.

5.3. The Ionization of N V

The small values of $\langle q(\text{N V}) \rangle$ and the presence of wind lines from an excited level of N IV* suggests that N IV is the dominant stage of ionization of N in the winds of O stars. The ionization potential of N IV is 77.5 eV, so the ionizing continuum is at $\lambda < 160 \text{ \AA}$. The ionization of N V is probably partly due to the radiative ionization from N IV* by stellar radiation, and partly due to ionization by shock-produced X-rays and collisional ionization in shocks (Pauldrach et al. 1994; MacFarlane et al. 1994). Therefore,

we do not expect that the ionization fraction of N V can be calculated by the nebular approximation. Nevertheless, we can try to describe the empirical ionization fractions of N V in terms of an expression similar to equation (18), but with an *empirical ionization temperature*.

Assuming that N IV is the dominant stage of ionization, and that the ratio N IV/N V can be described by equation (18), we can derive an expression for the column density of N V,

$$N(\text{N V}) = 6.30 \times 10^{26} R_* \frac{\rho}{n_e} \frac{n(\text{N})}{\rho} \sqrt{T_e} f_{\text{rad}}(\text{N V}) I_2, \quad (24)$$

where

$$f_{\text{rad}}(\text{N V}) = T_{\text{rad}}(\text{N V}) e^{-8.994 \times 10^5 / T_{\text{rad}}(\text{N V})} \quad (25)$$

and

$$I_2 = \int_{x(w=0.2)}^{\infty} W(x) dx. \quad (26)$$

Note that the mass-loss rate does not appear in equation (24). This is because the ionization fraction $\langle q(\text{N V}) \rangle$ is inversely proportional to ρ , i.e., proportional to v_{∞}/\dot{M} , but the column density is proportional to $\langle q(\text{N V}) \rangle \dot{M}/v_{\infty}$.

The empirical values of T_{rad} , derived from the observed column densities, are plotted versus T_{eff} in Figure 6a. The data show a surprisingly tight relation. A least-square fit gives the relation

$$\begin{aligned} \frac{T_{\text{rad}}(\text{N V})}{T_{\text{eff}}} = & 4.492 - 10.380 \left(\frac{T_{\text{eff}}}{40,000} \right) + 9.754 \left(\frac{T_{\text{eff}}}{40,000} \right)^2 \\ & - 3.175 \left(\frac{T_{\text{eff}}}{40,000} \right)^3. \end{aligned} \quad (27)$$

This relation fits the data very accurately within $\Delta T_{\text{rad}}/T_{\text{eff}} = 0.011$ (1σ). It is valid in the temperature range of $28,000 \text{ K} < T_{\text{eff}} < 51,000 \text{ K}$. The upper and lower limits agree with this relation, within their uncertainty. The resulting predicted values of $f_{\text{rad}}(\text{N V})$ are compared with those derived from the observed column densities in Figure 6b. The deviations are $1 \sigma \approx 0.2$ dex.

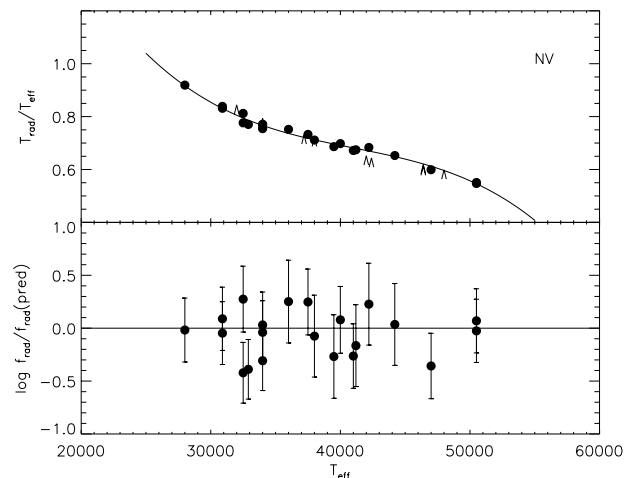


FIG. 6.—*Top*: ratio $T_{\text{rad}}/T_{\text{eff}}$ of N V as a function of T_{eff} . The solid line shows the best-fit cubic relation. *Bottom*: ratio between the empirical value of f_{rad} and the one predicted by the best-fit relation in the top figure.

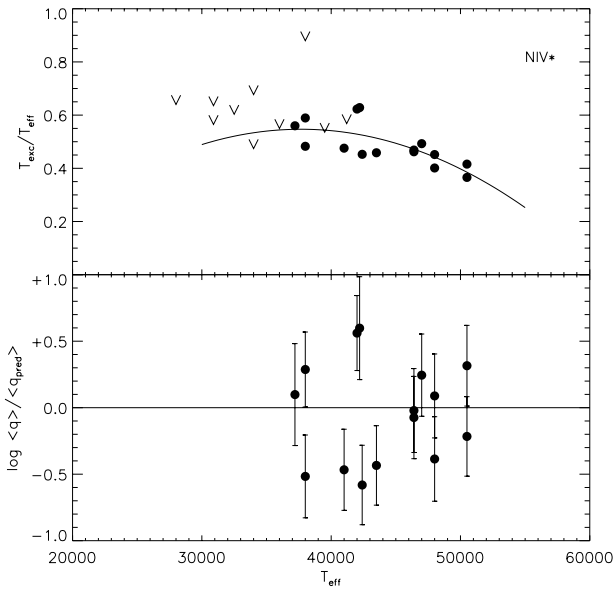


FIG. 7.—*Top*: ratio $T_{\text{exc}}/T_{\text{eff}}$ of N IV* as a function of T_{eff} . The solid line shows the best-fit quadratic relation. *Bottom*: ratio between the empirical value of $\log \langle q \rangle$ and the one predicted by the best-fit relation in the top figure.

The very tight relation between $T_{\text{rad}}/T_{\text{eff}}$ and T_{eff} in Figure 6a is partly due to the high ionization potential of N IV*, 77.5 eV. It is easy to see that for $T_{\text{rad}} \simeq 40,000$ K, the scatter in T_{rad} is $(\Delta T_{\text{rad}})/T_{\text{rad}} \simeq 0.10 \Delta \log \langle q(\text{N v}) \rangle$. Therefore, the very tight relation between T_{rad} and T_{eff} reflects the tight relation between the ionization fraction and the stellar parameters.

5.4. The Ionization and Excitation of N IV*

The presence of subordinate N IV* wind lines in the spectra of O stars with $37,000 \text{ K} < T_{\text{eff}} < 51,000 \text{ K}$ shows that N IV is the dominant ionization stage of N. The line at 1718 \AA comes from a lower level with an excitation energy of 16.21 eV. We express the excitation fraction in terms of an empirical excitation temperature, by means of the Boltzmann equation:

$$\frac{n(\text{N IV}^*)}{n(\text{N})} = \langle q(\text{N IV}^*) \rangle = \frac{g_l}{g_0} e^{-\chi_{\text{exc}}/kT_{\text{exc}}}, \quad (28)$$

with the statistical weights of the ground state and the lower level of the transition $g_0 = 1$ and $g_l = 1$, respectively, and $\chi_{\text{exc}} = 16.21 \text{ eV}$.

We found that the empirical excitation temperatures can be fitted to a simple quadratic function of T_{eff} :

$$\frac{T_{\text{exc}}}{T_{\text{eff}}} = -0.844 + 2.954 \left(\frac{T_{\text{eff}}}{40,000} \right) - 1.569 \left(\frac{T_{\text{eff}}}{40,000} \right)^2. \quad (29)$$

The values of $T_{\text{exc}}/T_{\text{eff}}$ are plotted versus T_{eff} in Figure 7a. The ratio decreases from about 0.6 near 40,000 K to 0.4 near 50,000 K. In Figure 7b, the empirical values of $\langle q(\text{N IV}^*) \rangle$ are compared with the ones predicted by equation (28). The scatter is 0.26 dex (1σ). The mass-loss rates derived from the N IV* line are proportional to $\langle q \rangle$, so they

will have the same uncertainty if the stellar parameters are accurately known.

5.5. The Ionization and Excitation of C III*

The C III* line at 1176 \AA comes from an energy level with an excitation potential of 6.50 eV. The population of this level depends on the ionization balance and the excitation balance. The dominant stage of ionization is expected to be C V for early O stars and C IV for late O stars (Pauldrach et al. 1994; de Koter 1993), so we cannot expect the population of the C III* level to be expressed as a simple dependence on an ionization and excitation temperature. Therefore, we decided to express the mean ionization and excitation fraction directly in terms of a quadratic function of T_{eff} , which fits the data satisfactorily. The least-square fit of the empirical values of $\langle q(\text{C III}^*) \rangle$ yields

$$\log \langle q(\text{C III}^*) \rangle = 0.265 - 7.567 \left(\frac{T_{\text{eff}}}{40,000} \right) + 4.071 \left(\frac{T_{\text{eff}}}{40,000} \right)^2. \quad (30)$$

This expression is valid in the temperature range of $28,000 \text{ K} < T_{\text{eff}} < 42,000 \text{ K}$. The upper and lower limits roughly agree with it.

Figure 8b shows the comparison between the empirical values of $\langle q(\text{C III}^*) \rangle$ and the predicted ones. The scatter is 0.14 dex (1σ). The upper part of this figure shows the excitation temperature defined by the Saha-Boltzmann equation if we assume that C IV is the dominant stage of ionization in the winds where we observe C III* wind lines:

$$\langle q(\text{C III}^*) \rangle \simeq \frac{n(\text{C III}^*)}{n(\text{C})} \simeq \frac{g_l}{2U(\text{C IV})} \left(\frac{h^2}{2\pi m_e k} \right)^{3/2} \times \frac{n_e}{\sqrt{T_e T_{\text{rad}}}} e^{+\chi/kT_{\text{rad}}}, \quad (31)$$

where $g_l = 1$ is the statistical weight of the lower level of the observed transition and $U(\text{C IV}) = 2$ is that of the C IV ground level. In this expression, $\chi = 47.89 - 6.50 = 42.39 \text{ eV}$ is the energy difference between the lower level of the transition and the ionization of C IV. The excitation tem-

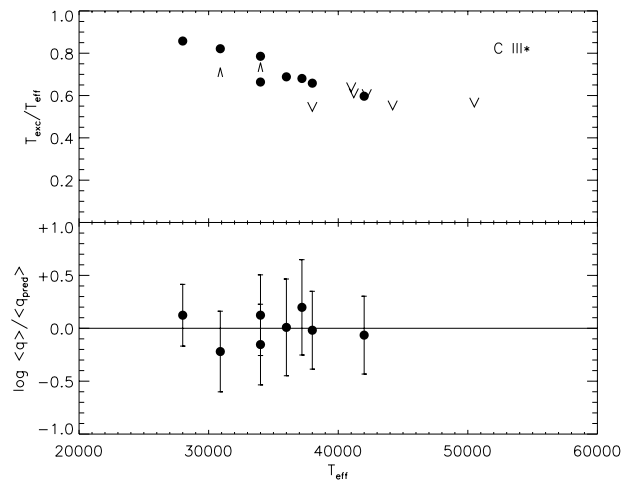


FIG. 8.—*Top*: ratio $T_{\text{exc}}/T_{\text{eff}}$ of C III* as a function of T_{eff} . We do not show the best-fit relation because it depends on both T_{eff} and $\langle \rho \rangle$. *Bottom*: ratio between the empirical ionization fraction and the one predicted by the best fit of T_{exc} .

perature decreases from about $0.9 T_{\text{eff}}$ near 28,000 K to $0.6 T_{\text{eff}}$ near 42,000 K.

6. DETERMINING MASS-LOSS RATES FROM UV LINES

With the ionization and excitation relations derived in the previous section, one can derive the mass-loss rates of O stars from the column density of the observed ions.

The mass-loss rate derived from the Si IV lines is given by

$$\dot{M}^2(\text{Si IV}) = \frac{N(\text{Si IV})}{3.09 \times 10^{-9}} \left(\frac{\rho}{n_e} \right) \left(\frac{\rho}{n_{\text{Si}}} \right) \frac{R_*^3 v_\infty^2}{I - 1} \sqrt{0.8 T_{\text{eff}}} \\ \times T_{\text{rad}}(\text{Si IV}) e^{-5.238 \times 10^5 / T_{\text{rad}}(\text{Si IV})}, \quad (32)$$

where $T_{\text{rad}}(\text{Si IV})$ is given by equation (22). The relation is valid in the range of $27,000 \text{ K} \leq T_{\text{eff}} \leq 48,000 \text{ K}$.

The mass-loss rate derived from the C IV lines is

$$\dot{M}(\text{C IV}) = \frac{N(\text{C IV})}{7.20 \times 10^{+8}} \left(\frac{\rho}{n_C} \right) \frac{R_* v_\infty}{I_3} \frac{1}{\langle q(\text{C IV}) \rangle}. \quad (33)$$

This equation is only valid for $32,000 \text{ K} \leq T_{\text{eff}} \leq 40,000 \text{ K}$ and $\log \langle \rho \rangle \leq -14.0$.

The mass-loss rate derived from the N IV* line is

$$\dot{M}(\text{N IV}^*) = \frac{N(\text{N IV}^*)}{7.20 \times 10^{+8}} \left(\frac{\rho}{n_N} \right)^{-1} \frac{R_* v_\infty}{I_3} \\ \times e^{-8.990 \times 10^5 / T_{\text{rad}}(\text{N IV}^*)}, \quad (34)$$

where $T_{\text{rad}}(\text{N IV}^*)$ is given by equation (29) and I_3 is

$$I_3 = \int_{x(w=0.2)}^{\infty} \frac{dx}{wx^2}. \quad (35)$$

The relation is valid in the range of $38,000 \text{ K} \leq T_{\text{eff}} \leq 52,000 \text{ K}$.

The mass-loss rate derived from the C III* line is

$$\dot{M}(\text{C III}^*) = \frac{N(\text{C III}^*)}{7.20 \times 10^{+8}} \left(\frac{\rho}{n_C} \right) \frac{R_* v_\infty}{I_3} \frac{1}{\langle q(\text{C III}^*) \rangle}, \quad (36)$$

where $\langle q(\text{C III}^*) \rangle$ is given by equation (31). The relation is valid in the range of $28,000 \text{ K} \leq T_{\text{eff}} \leq 42,000 \text{ K}$.

The mass-loss rate cannot be derived from the N V lines, because the column density of N V is independent of the mass-loss rate. All relations are only valid for stars with mass-loss rates in the range $-7.5 M_\odot \text{ yr}^{-1} \lesssim \log \dot{M} \lesssim -4.7 M_\odot \text{ yr}^{-1}$.

7. A CONSISTENCY CHECK

To test the consistency of our empirical ionization fractions, we have derived the mass-loss rates of the program stars from the UV lines as described above and compared this with the input mass-loss rates derived from the radio flux and from H α . Obviously, this test is partly circular, because we have used the same mass-loss rates to derive the ionization relations. However, it is a valid test to check the differences in the mass-loss rates derived from each ion individually. It is also used to compare the mass-loss rates derived from the UV lines for three stars that have new mass loss determinations from radio fluxes.

The result is given in Table 4, which gives the values of \dot{M} derived from each line. We also give the mean value derived from the four ions and the resulting value of σ . If the mass-

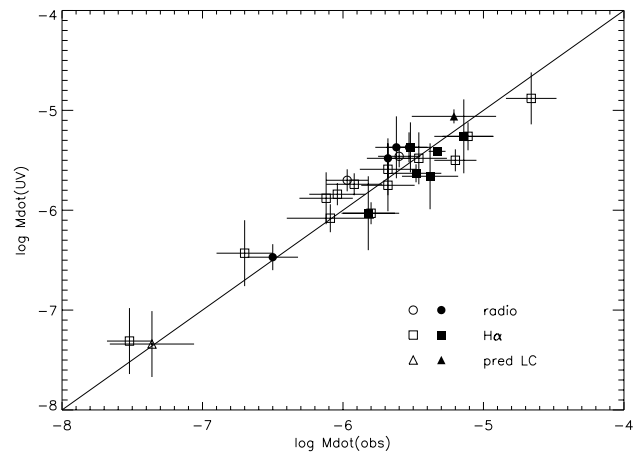


FIG. 9.—Comparison of the mass-loss rates derived from the UV lines by means of the ionization and excitation relations derived in § 5 with the rates $\dot{M}(\text{obs})$ derived from the radio flux (circles), H α (squares), or from the relation of Lamers & Cassinelli (1996) (triangles). Filled and open symbols indicate mass-loss rates derived from more than one ion or from one ion, respectively.

loss rate could be determined from only one ion, the uncertainty is the value of σ for that particular ion, as given in § 5. For HD 93250 and HD 101190, we could not derive a mass-loss rate from the UV lines because the different ions give conflicting results. In particular, the upper limit of the mass-loss rate derived from the C III* line disagrees with the other values. We recall that the C III* lines are in a very noisy part of the IUE spectrum. A study based on higher S/N ratio spectra may solve this problem.

The last two columns of Table 4 give the mass-loss rates derived from the radio flux or from H α and the difference between these observed rates and those derived from the UV lines. These differences are typically smaller than 0.30.

There is one exception: HD 190429 (O4 f⁺). For this star, the mass-loss rates derived from the Si IV and N IV* lines both suggest $\log \dot{M} = -5.4$, whereas the rate derived from H α by LL, with the correction from Puls et al. (1995), suggests a much higher value of -4.86 . After this study was finished, Scuderi et al. (1998) published a new mass-loss rate of $\log \dot{M} = -5.33 \pm 0.06$ for this star, based on new radio flux measurements. This agrees very well with our determination based on UV lines, thus supporting our results. For HD 14947, Scuderi et al. (1998) derived $\log \dot{M} = -5.52 \pm 0.12$. Our value of -5.37 also agrees better with this new radio rate than with the value of -5.12 derived from H α . For the third star in common with Scuderi et al., HD 37128, the new radio rate of -5.68 ± 0.07 is smaller than the rate of -5.37 ± 0.15 derived from the UV lines, but is also smaller than the rate of -5.39 ± 0.16 derived from previous radio observations (see Table 1).

The rates derived from the UV lines are plotted versus the observed mass-loss rates in Figure 9. For this figure, we adopted the new radio mass-loss rates from Scuderi et al. (1998) for HD 14947 and HD 190429, and the mean value of the two radio rates for HD 37128. Note that the data agree within the accuracies. This shows that the mass-loss rates can be derived from the UV lines with an accuracy that depends on the number of ions that can be used, but with a typical uncertainty of about a factor of 2, if the stellar parameters are accurately known and the column densities are derived accurately from the UV lines. Uncertainties in

TABLE 4
 MASS-LOSS RATES DERIVED FROM THE OBSERVED P CYGNI PROFILES WITH THE EMPIRICAL IONIZATION FRACTIONS

HD	log \dot{M}				Mean	Observed	$\Delta \log \dot{M}$
	C IV	Si IV	N IV*	C III*			
14947	-5.19	-5.55	...	-5.37 ± 0.25	-5.12 ± 0.18	-0.25 ^b
15558	-5.00	-5.53	...	-5.26 ± 0.37	-5.14 ± 0.21	-0.12
15570	< -5.48	< -5.48 ± 0.22	-5.33 ± 0.18	...
15629	< -5.45	-5.88	...	-5.88 ± 0.26	-6.12 ± 0.19	+0.24
36486	-5.70	-5.70 ± 0.11	-5.97 ± 0.15	+0.27
36861	< -6.26	< -6.04	-6.08	-6.08 ± 0.14	-6.09 ± 0.31	+0.01
37043	-6.56	< -6.11	< -5.54	-6.37	-6.47 ± 0.13	-6.50 ± 0.18	+0.03
37128	-5.47	< -3.54	-5.26	-5.37 ± 0.15	-5.39 ± 0.16	+0.02 ^b
37742	-5.46	< -4.49	> -5.08	-5.46 ± 0.11	-5.60 ± 0.15	+0.14
46223	< -5.72	-5.75	...	-5.75 ± 0.26	-5.68 ± 0.19	-0.07
47839	< -6.33	< -6.24	...	< -6.28 ± 0.15	-6.19 ± 0.31	...
57061	-5.50	-5.50 ± 0.11	-5.20 ± 0.15	-0.30
66811	-5.37	-5.06	-5.68	-5.37 ± 0.31	-5.62 ± 0.15	+0.25
93129	< -4.95	-4.88	...	-4.88 ± 0.26	-4.66 ± 0.18	-0.22
93204	< -5.95	...	< -6.61	< -6.61 ± 0.14	-6.55 ± 0.30 ^a	...
93250	< -5.00	-4.99	< -6.52	...	-5.31 ± 0.18	+0.32
101190	< -5.78	-5.45	< -6.35	...	-6.05 ± 0.30 ^a	+0.60
101413	-7.34	< -6.24	< -5.87	< -6.45	-7.34 ± 0.33	-7.36 ± 0.30 ^a	+0.02
101436	< -5.93	< -6.01	< -6.40	< -6.11 ± 0.25	-6.23 ± 0.30 ^a	...
149038	-5.57	< -4.89	-5.70	-5.63 ± 0.09	-5.48 ± 0.18	-0.15
149404	> -4.99	> -4.99 ± 0.11	-4.91 ± 0.15	...
149757	-7.31	-7.31 ± 0.33	-7.52 ± 0.16	+0.21
151804	> -5.16	...	> -4.94	> -5.00 ± 0.16	-5.00 ± 0.17	...
163758	> -5.06	-5.11	-5.01	-5.06 ± 0.07	-5.21 ± 0.30 ^a	+0.15
164794	< -5.44	-5.48	...	-5.48 ± 0.26	-5.46 ± 0.20	-0.02
188001	> -5.29	< -5.67	-5.26	-5.26 ± 0.14	-5.11 ± 0.18	-0.15
190429	-5.38	-5.44	...	-5.41 ± 0.04	-4.86 ± 0.18	-0.55 ^b
190864	-5.76	-6.29	< -6.07	-6.03 ± 0.37	-5.82 ± 0.19	-0.21
193514	-5.43	-5.90	...	-5.66 ± 0.33	-5.38 ± 0.20	-0.28
203064	-5.74	-5.74 ± 0.11	-5.92 ± 0.20	+0.18
207198	-6.03	-6.03 ± 0.11	-5.80 ± 0.20	-0.23
209975	-5.84	< -5.38	...	-5.84 ± 0.11	-6.04 ± 0.20	+0.20
210839	-5.33	-5.39	-5.70	-5.48 ± 0.20	-5.68 ± 0.15	+0.20
217086	-6.43	-6.43 ± 0.33	-6.70 ± 0.20	+0.27
303308	< -5.47	-5.59	...	-5.59 ± 0.26	-5.68 ± 0.20	+0.09

^a Predicted mass-loss rate from the relation by Lamers & Cassinelli (1996).

^b See § 7.

R_* , v_∞ , the column density, and the abundances also affect the accuracy of the derived mass loss, because $\dot{M} \sim R_* v_\infty N_i / A_E$.

8. SUMMARY AND CONCLUSIONS

We have derived empirical mean ionization fractions $\langle q(\text{C IV}) \rangle$, $\langle q(\text{N V}) \rangle$, and $\langle q(\text{Si IV}) \rangle$, and mean ionization and excitation fractions $\langle q(\text{C III}^*) \rangle$ and $\langle q(\text{N IV}^*) \rangle$ in the winds of O stars by comparing the optical depth of the P Cygni profiles with the mass-loss rates derived from different methods, i.e., from H α and from the radio free-free flux. Our analysis is hampered by the lack of accurate abundances of C and N in most stars. We adopted mean C/N ratios per spectral type or luminosity class, derived from detailed studies of a few stars. The mean ionization and excitation fractions are plotted versus T_{eff} and the mean wind density $\langle \rho \rangle$ in Figures 3 and 4.

The mean ionization fractions or column densities can be expressed in terms of simple relations, using the expected modified Boltzmann and Saha equations with empirically derived values of the radiation temperatures. These radiation temperatures depend on T_{eff} . We derived these rela-

tions from least-square fits. The fits are described in § 5 and shown in Figures 5–8. For C IV, we could derive a relation between the mean ionization fraction only in the range of $32,000 \text{ K} \leq T_{\text{eff}} \leq 40,000 \text{ K}$ and for a mean wind density of $\log \log \langle \rho \rangle < -14.10$, which corresponds to mass-loss rates smaller than about $10^{-6} M_\odot \text{ yr}^{-1}$. This is because the C IV lines are mostly saturated for higher mass-loss rates.

Using these empirical fits, one can derive the mass-loss rates of O stars from the UV resonance lines of C IV, Si IV, N IV*, and C III*. The Si IV lines give the most accurate mass-loss rates. This is due to four effects: (1) the abundance of Si is about the same in all O stars; (2) the lines saturate only in stars with very high mass-loss rates, because of the low abundance; (3) the line fits of the Si IV lines are quite accurate, because the profiles of the two doublet lines overlap only partly; and (4) the mass-loss rate depends on the square root of the column density. It turns out that the column densities derived from the N V resonance lines are independent of the mass-loss rate, because the ionization fraction depends on ρ^{-1} . This is expected for winds in which N IV is the dominant stage of ionization. The empirical ionization fraction of N V shows a very strict correlation

with T_{eff} : $(\Delta T_{\text{rad}})/T_{\text{rad}} \simeq 0.011$, which corresponds to $\Delta \log \langle g(\text{N v}) \rangle \simeq 0.2$.

We have checked the consistency of the mass-loss determinations by using the derived empirical relations to the column densities of the observed ions in our program stars. We found that the fits reproduce the empirical mass-loss rates derived from the radio flux or from H α with an accuracy better than a factor of 2. The accuracy increases if the column densities of different ions can be used. We realize that this test is partly circular, because the empirical relations were derived from the same stars. However, the test is useful to search for mass-loss differences derived from different ions and to find deviating stars. Since we found rather smooth empirical relations between the ionization or excitation temperatures and the stellar parameters, we expect that they will also apply to other stars.

After this study was completed, Scuderi et al. (1998) published new mass-loss rates derived from radio flux mea-

surements. For one star, HD 37128, the new radio mass-loss rate, $\log \dot{M} = -5.68 \pm 0.07$, is a factor of 2 smaller than the previously measured radio mass-loss rate, listed in Table 1. Our results agree better with the previous radio mass-loss rate. For the other two stars in common with our program stars, HD 14749 ($\log \dot{M} = -5.52 \pm 0.11$) and HD 190429 ($\log \dot{M} = -5.34 \pm 0.06$), the radio flux was not measured previously. The mass-loss rates derived from the UV lines agree very well with the new radio rates, which strengthens our confidence in our results.

H. J. G. L. M. L. is grateful to the Space Telescope Science Institute for support and hospitality. We thank Nolan Walborn for comments on the spectral types of the program stars. A. de K. gratefully acknowledges financial support from NASA Astrophysics Data Program NRA 95-ADP-09 and from an NWO "Pionier" grant to L. Waters.

REFERENCES

- de Koter, A. 1993, Ph.D. thesis, Univ. Utrecht
 Groenewegen, M. A. T., & Lamers, H. J. G. L. M. 1989, *A&AS*, 79, 359 (GL)
 ———, 1991, *A&A*, 243, 429
 Hamann, W. R. 1981, *A&A*, 93, 353
 Haser, S. 1995, Ph.D. thesis, Univ. Munich
 Herrero, A., Kudritzki, R. P., Vílchez, J. M., Kunze, D., Butler, K., & Haser, S. 1992, *A&A*, 261, 209
 Howarth, I. D., & Prinja, R. K. 1989, *ApJS*, 69, 527
 Lamers, H. J. G. L. M., & Cassinelli, J. P. 1996, in *ASP Conf. Ser. 98, From Stars to Galaxies: The Impact of Stellar Physics on Galaxy Evolution*, ed. C. Leitherer, U. Fritze-von Alvensleben, & J. Huchra (San Francisco: ASP), 162
 Lamers, H. J. G. L. M., Cerruti-Sola, M., & Perinotto, M. 1987, *ApJ*, 314, 726
 Lamers, H. J. G. L. M., Gathier, R., & Snow, T. P. 1980, *ApJ*, 242, L33
 Lamers, H. J. G. L. M., & Leitherer, C. 1993, *ApJ*, 412, 771
 Lamers, H. J. G. L. M., Snow, T. P., & Lindholm, D. M. 1995, *ApJ*, 455, 269
 Lennon, D. J., Kudritzki, R. P., Becker, S. T., Butler, K., Eber, F., Groth, H. G., & Kunze, D. 1991, *A&A*, 252, 498
 MacFarlane, J. J., Cohen, D. H., & Wang, P. 1994, *ApJ*, 437, 351
 MacFarlane, J. J., Waldron, W. L., Corcoran, M. F., Wolff, M. J., Wang, P., & Cassinelli, J. P. 1993, *ApJ*, 419, 813
 Maeder, A. 1990, *A&AS*, 84, 139
 Mihalas, D. 1970, *Stellar Atmospheres* (San Francisco: Freeman)
 Pauldrach, A. W. A., Kudritzki, R. P., Puls, J., Butler, K., & Hunsinger J. 1994, *A&A*, 283, 525
 Pauldrach, A. W. A., Puls, J., & Kudritzki, R. P. 1986, *A&A*, 164, 86
 Puls, J., et al. 1995, *A&A*, 305, 171
 Schönberner, D., Herrero, A., Becker, S., Eber, F., Butler, K., Kudritzki, R. P., & Simon, K. P. 1988, *A&A*, 197, 209
 Scuderi, S., Panagia, N., Stanghellini, C., Trigilio, C., & Umana, G. 1998, *ApJ*, submitted
 Snow, T. P., Lamers, H. J. G. L. M., Lindholm, D. M., & Odell, A. P. 1994, *ApJS*, 95, 163
 Snow, T. P., & Morton, D. C. 1976, *ApJS*, 32, 429
 Voels, S. A., Bohannan, B., Abbott, D. C., & Hummer, D. G. 1989, *ApJ*, 340, 1073
 Walborn, N. R. 1976, *ApJ*, 205, 419
 ———, 1988, in *IAU Colloq. 108, Atmospheric Diagnostics of Stellar Evolution*, ed. K. Nomoto (Berlin: Springer), 70